Journal of the Korea Convergence Society
Vol. 8. No. 5, pp. 1-11, 2017
https://doi.org/10.15207/JKCS.2017.8.5.001

The Control of Spring-Mass-Damper Convergence System using H_∞ Controller and μ - Synthesis Controller

Sunghun Jung
Department of Drone System, Chodang University

H_∞ 제어와 μ-합성 제어를 이용한 스프링-질량-감쇠 융합시스템 제어

정성훈
초당대학교 항공학부 드론학과

Abstract With a given spring-mass-damper system, H_∞ and μ-synthesis control methods are used to build system controllers which minimize vibrations at two major natural frequencies in two cases; without uncertainty; with 20% uncertainty. In order to check the stability and performance of two controllers, those are examined using GM and PM values. The signal strength of output responses is compared using the concept of central numerical differentiation and then results are quantified using the RMS method. Lastly, 40 random samples of H_∞ and μ-synthesis controllers are obtained for three different W_{perf1} weighting functions and drawn in the time domain in order to compare the stability. Overall, μ-synthesis controller manages the vibrations much better than H_∞ controller according to the robust stability and performance values obtained by simulating random samples of 40 plant models.

• Key Words : CLTF, H-Infinity, Mu-Synthesis, RMS, TF

요 약 H_∞ 제어와 뮤-합성 제어 방법을 사용하여 두 가지 상황, 즉 불확실성이 포함되지 않았을 때와 20% 불확실성이 포함되었을 때, 하에서 스프링-매스-댐퍼 시스템의 진동을 최소화하였다. 두 컨트롤러의 안정성 및 성능 파악을 위해 GM와 PM 값을 사용하여 분석되었다. 중앙 수치 미분법과 RMS 방법을 사용하여 출력 응답의 신호 강도가 비교되었다. 끝으로, 안정성 비교를 위하여 3가지 다른 W_{perf1} 가중함수의 경우에 대해 총 40개의 H_∞ 제어기와 뮤-합성 제어기 무작위 표본이 생성되었다. 전반적으로, 40개 플랜트 모델에서 얻어진 결과 값의 견고한 안정성과 성능 값에 따르면, 뮤-합성 제어기가 H_∞ 제어기보다 진동 관리에 효과적임이 입증되었다

• 주제어 : CLTF, H-Infinity, Mu-합성, 제곱평균제곱근, 전달함수

1. Introduction

Exact control of electrical, mechanical, and even mechatronical system components is getting important due to the increased complexities of recently developed systems in the domains of such as automotive, aerospace, civil, and etc.

*Corresponding Author : 정성훈(jungx148@gmail.com)
Received February 14, 2017 Revised March 14, 2017
Accepted May 20, 2017 Published May 28, 2017

Among hundreds and thousands of components configuring a system, a spring- mass-damper component is one of the most widely applied system component [1]. There are many approaches to control a spring-mass- damper system for automotive applications, including model predictive control (MPC) [2,3] and semiactive force generators [4] and it is even applied to civil engineering structures including magnetorheological (MR) dampers [5,6], semiactive tuned mass damper (TMD) [7], semiactive variable stiffness tuned mass damper (SAIVS-TMD) [8], and tuned liquid column damper [9].

There are several reasons why output feedback (OPFB) is preferred than state variable feedback (SVFB); firstly, static OPFB controllers cost less than the full SVFB controllers most of the time; secondly, it is not possible to observe all state vectors for the feedback in real life; thirdly, static OPFB has a sturdier structure than SVFB; finally, static OPFB is often used as a backup controller which only operates when there is a system failure [10,11].

In this paper, disturbance attenuation and system control will be discussed in the prescribed performance using H_∞ loop shaping method and μ-synthesis method at both the first and the second natural frequencies [12,13,14]. In addition, loop shaping method will be studied for getting better disturbance rejections.

The flow of this paper is as follows. Section 2 shows an overview of the spring-mass- damper system and Section 3 describes the system model. Section 4 illustrates H_∞ controller design with no uncertainty and Section 5 illustrates μ-synthesis controller design with 20% uncertainty involvement. Lastly, Section 6 contains the conclusion of this paper and future works.

2. System Overview

The overall system is shown in [Fig. 1] and free body diagram is shown in [Fig. 2] [15,16]. Inputs, an output, and an uncertainty level are shown in <Table 1>.

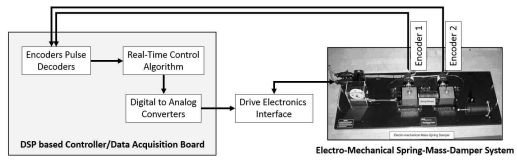

[Fig. 1] Overall spring-mass-damper system [14]

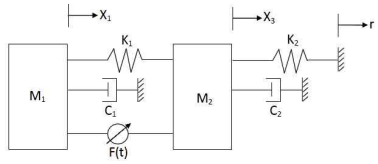

[Fig. 2] Free body diagram of the two degrees of freedom spring-mass-damper system

<Table 1> Input, output, and uncertainty level of the spring-mass-damper system

Control Input	F
External Input	r
Disturbance Input	$d_1,\ d_2$
Output	$x_1, x_1 - x_3$
Uncertainty Level	20%

In [Fig. 2], an additional spring, k_2, on the right side of the mass, M_2, is attached to be compared to the original system.

The overall H_∞ control design is designed as shown in [Fig. 3] [17].

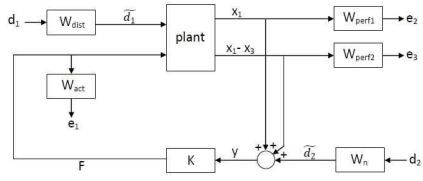

[Fig. 3] Block diagram of H_∞ controller

3. System Model

The dynamic equation of the given system model is,

$$m_1\ddot{x}_1(t)+c_1\dot{x}_1(t)+k_1(x_1(t)-x_3(t))=F(t),$$
$$m_2\ddot{x}_3(t)+c_2\dot{x}_3(t)+k_1(x_3(t)-x_1(t))+k_2(x_3(t)-r(t))=-F(t), \quad (1)$$

where $m_1 = 2.77kg$, $m_2 = 2.59kg$, $c_1 = 2.1N/(m/s)$, $c_2 = 1.2N/(m/s)$, $k_1 = 830N/m$, and $k_2 = 830N/m$.

As shown in Eq. 1, there are two inputs (r and F) and four outputs (x_1, $\dot{x}_1$, x_3, and F) and this multiple-input and multiple-output (MIMO) state space model can be rewritten in matrix forms as,

$$\begin{bmatrix} \dot{x}_1 \\ \ddot{x}_1 \\ \dot{x}_3 \\ \ddot{x}_3 \end{bmatrix} = \begin{bmatrix} 0 & 1 & 0 & 0 \\ -\frac{k_1}{m_1} & -\frac{c_1}{m_1} & \frac{k_1}{m_1} & 0 \\ 0 & 0 & 0 & 1 \\ \frac{k_1}{m_2} & 0 & -\frac{k_1+k_2}{m_2} & -\frac{c_2}{m_2} \end{bmatrix} \begin{bmatrix} x_1 \\ \dot{x}_1 \\ x_3 \\ \dot{x}_3 \end{bmatrix} + \begin{bmatrix} 0 & 0 \\ 0 & \frac{10000}{m_1} \\ 0 & 0 \\ \frac{k_2}{m_2} & -\frac{10000}{m_2} \end{bmatrix} \begin{bmatrix} r \\ F \end{bmatrix}, \quad (2)$$

$$\begin{bmatrix} x_1 \\ \ddot{x}_1 \\ x_3 \\ F \end{bmatrix} = \begin{bmatrix} 1 & 0 & 0 & 0 \\ -\frac{k_1}{m_1} & -\frac{c_1}{m_1} & \frac{k_1}{m_1} & 0 \\ 0 & 0 & 1 & 0 \\ 0 & 0 & 0 & 0 \end{bmatrix} \begin{bmatrix} x_1 \\ \dot{x}_1 \\ x_3 \\ \dot{x}_3 \end{bmatrix} + \begin{bmatrix} 0 & 0 \\ 0 & \frac{10000}{m_1} \\ 0 & 0 \\ 0 & 1 \end{bmatrix} \begin{bmatrix} r \\ F \end{bmatrix},$$

where A, B, C, and D matrices are defined as

$$A = \begin{bmatrix} 0 & 1 & 0 & 0 \\ -299.6390 & -0.7581 & 299.6390 & 0 \\ 0 & 0 & 0 & 1 \\ 320.4633 & 0 & -640.9266 & -0.4633 \end{bmatrix},$$

$$B = \begin{bmatrix} 0 & 0 \\ 0 & 3.6101 \\ 0 & 0 \\ 320.5 & -3.8610 \end{bmatrix},$$

$$C = \begin{bmatrix} 1 & 0 & 0 & 0 \\ -299.6390 & -0.7581 & 299.6390 & 0 \\ 0 & 0 & 1 & 0 \\ 0 & 0 & 0 & 0 \end{bmatrix},$$

$$D = \begin{bmatrix} 0 & 0 \\ 0 & 3610.1 \\ 0 & 0 \\ 0 & 1 \end{bmatrix}.$$

Using MATLAB, plant poles, zeros, and natural frequencies are obtained as shown in <Table 2>.

<Table 2> Plant poles, zeros, and natural frequencies of the system

Eigenvalue	Damping	Freq. (rad/s)
-3.41e-1 + 1.08e1i	3.16e-2	1.08e1
-3.41e-1 - 1.08e1i	3.16e-2	1.08e1
-2.70e-1 + 2.87e1i	9.40e-3	2.87e1
-2.70e-1 - 2.87e1i	9.40e-3	2.87e1

The [Fig. 4] illustrates calculated natural frequencies shown in <Table 2>. The first graph is obtained from the output y_1 and the second graph is come from the output $y_1 - y_3$ which is equal to the distance of $x_1 - x_3$.

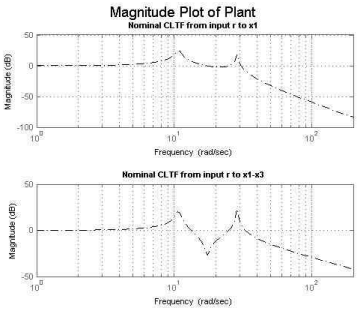

[Fig. 4] Bode plots of two outputs, x_1 and $x_1 - x_3$

4. H_∞ Controller Design (With No Uncertainty)

4.1 Motion Control of x_1

Two H_∞ controllers are designed and each controller is named as K_1 and K_2 where those were designed first and second, respectively.

4.2 Selection of Weighting TFs

By assuming that a sensor noise value of 0.01 m and the maximum vibration of 0.01 m ($r(t)$ which is applied to the spring, k_2), we can set $W_n = 0.01$ and $W_{dist} = 0.01$.

Then, weighting transfer functions (TF) are chosen based on the rigorous consideration as shown in Eq. 3 and [Fig. 5].

$$W_{act} = 10\frac{s+40}{s+400}, \quad (3)$$
$$W_{perf1} = 6\frac{20\pi}{s+20\pi},$$
$$W_{perf2} = 30\frac{80}{s+80}.$$

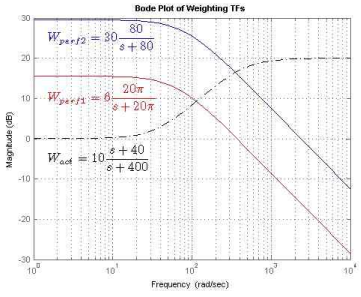

[Fig. 5] Bode plot of weighting TFs

After choosing all weighting TFs, an augmented system is built using a MATLAB command, *sysic*, as shown in Eq. 4. The augmented system has seven states, three outputs (W_{act}, W_{perf1}, and $x_1 - x_3 + W_n$), and three inputs (d_1, d_2, and F).

$$\dot{x}_{aug}(t) = A_{aug}x_{aug}(t) + B_{aug}u_{aug}(t), \quad (4)$$
$$y_{aug}(t) = C_{aug}x_{aug}(t) + D_{aug}u_{aug}(t),$$

where

$$A_{aug} = \begin{bmatrix} 0 & 1 & 0 & 0 & 0 & 0 & 0 \\ -299.6 & -0.7581 & 299.6 & 0 & 0 & 0 & 0 \\ 0 & 0 & 0 & 1 & 0 & 0 & 0 \\ 320.5 & 0 & -640.9 & -0.4633 & 0 & 0 & 0 \\ 0 & 0 & 0 & 0 & -400 & 0 & 0 \\ 16 & 0 & 0 & 0 & 0 & -62.83 & 0 \\ 0 & 0 & 64 & 0 & 0 & 0 & -80 \end{bmatrix},$$

$$B_{aug} = \begin{bmatrix} 0 & 0 & 0 \\ 0 & 0 & 3.61 \\ 0 & 0 & 0 \\ 3.205 & 0 & -3.861 \\ 0 & 0 & 64 \\ 0 & 0 & 0 \\ 0 & 0 & 0 \end{bmatrix},$$

$$C_{aug} = \begin{bmatrix} 0 & 0 & 0 & 0 & -56.25 & 0 & 0 \\ 0 & 0 & 0 & 0 & 0 & 23.56 & 0 \\ 1 & 0 & -1 & 0 & 0 & 0 & 0 \end{bmatrix},$$

$$D_{aug} = \begin{bmatrix} 0 & 0 & 10 \\ 0 & 0 & 0 \\ 0 & 0.01 & 0 \end{bmatrix}.$$

4.3 H∞ Controller Design to Minimize $x_1 - x_3$

The H_∞ controller is designed using MATLAB and [Fig 6] shows the responses of the plant, CL_1, and CL_2 when $r(t)$ is applied to m_2. Again, the K_1 controller is designed first and K_2 controller is designed later. It shows that the K_2 controller works much better than the K_1 controller which only works well with the first peak.

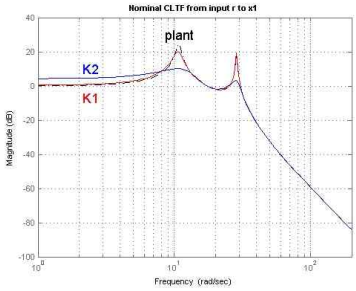

(a) Closed loop TFs for minimizing x_1

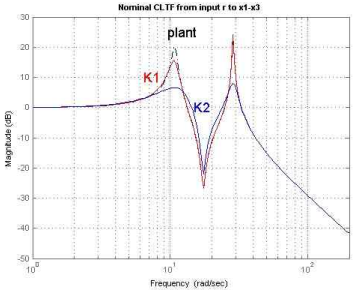

(b) Closed loop TFs for minimizing $x_1 - x_3$

[Fig. 6] Closed loop TFs for minimizing x_1 and $x_1 - x_3$

In order to verify the stability of both K_1 and K_2 controllers, gain margin (GM) and phase margin (PM) values are calculated using a MATLAB command, *margin*, as shown in <Table 3> and [Fig. 7].

<Table 3> PM and GM values of plant, CL_1, and CL_2

	Plant	CL_1	CL_2
GM (*dB*)	Inf	Inf	Inf
PH (*deg*)	3.43	2.56	11.7

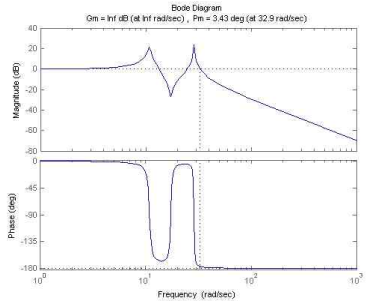

(a) Bode plot of plant

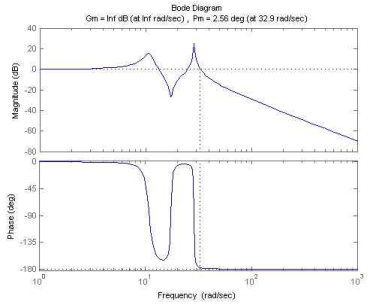

(b) Bode plot of CL_1

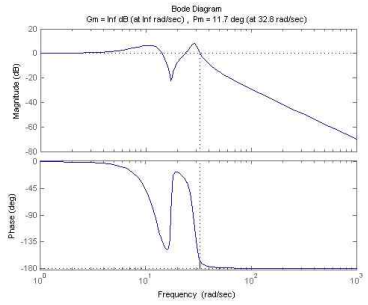

(c) Bode plot of CL_2

[Fig. 7] Bode plots of plant, CL_1, and CL_2

Since all GM values are larger than one and PM values are nonnegative, it can be considered as stable. Though CL_1 has lower PM value than plant, it is improved with the second CL_2 design which shows the much higher PM value, 11.7 *deg*.

The [Fig. 8] shows all responses including x_1, $\ddot{x}_1$, x_3, and F. According to the third graph in [Fig. 8], it is obvious that the K_2 works greatly compared to the K_1 which behaves almost same with the plant. The K_1 (H_∞ controller) achieved a norm of 0.85139 and K_2 (μ-synthesis controller) achieved a norm of 1.294 which are quite close to one.

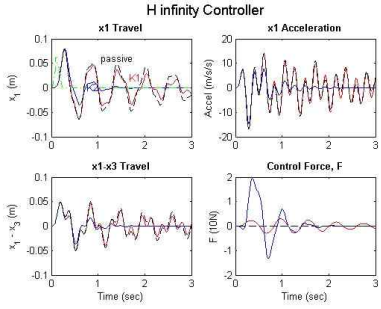

(a) System responses of x_1, $\ddot{x}_1$, x_3, and F

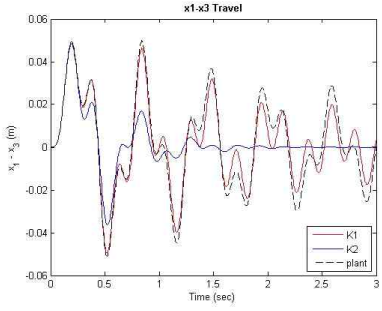

(b) System response of $x_1 - x_3$

[Fig. 8] System responses of H_∞ controller

In order to compare the signal strength of three vibrations in detail, the third figure of [Fig. 8(a)] is redrawn in [Fig. 8(b)]. Using the concept of central numerical differentiation and root mean square (RMS), acceleration data are used to quantify the strength of the vibration where acceleration data are usually used to quantify the signal strength by most jurisdictions and standard agencies. According to [18], a central difference for higher order derivative is defined as,

$$f''(x_i) = y'' \simeq \frac{y_{i+1} - 2y_i + y_{i-1}}{h^2} \tag{5}$$

where y'' is the acceleration, y_i is the result data, and h is the time interval.

In addition, RMS value of a set of values is the square of the arithmetic average of the squares of the original values. Equation of the RMS when there is a set of n values, x_1, ..., x_n, is defines as

$$x_s = \sqrt{\frac{x_1^2 + x_2^2 + \ldots + x_n^2}{n}} \quad (6)$$

and the result of the RMS values is shown in <Table 4>.

<Table 4> PM and GM values of plant, CL_1, and CL_2

	Plant	CL_1	CL_2
RMS	8.4130	8.7654	3.9860

According to <Table 4>, CL_2 has the lowest RMS value, 3.9860, and it means that the vibration is the lowest among three curves shown in [Fig. 8(b)]. The K_1, however, turns out to be even worse than the original plant.

5. μ-Synthesis Controller Design (With 20% Uncertainty)

In this section, 20% of uncertainty is introduced into the system. In order to control the uncertainty, μ-synthesis controller is newly designed and shown in [Fig. 9].

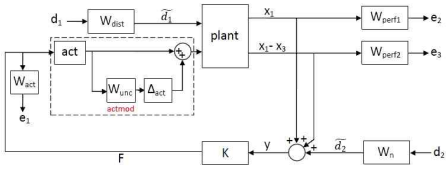

[Fig. 9] Block diagram of μ-synthesis controller

According to the actuator uncertainty weighting TF designed as

$$W_{unc} = 0.2\frac{\frac{1}{4}s+1}{\frac{1}{3000}s+1} \quad (7)$$

and shown in [Fig. 10], there is 20% vibration at lower frequency and it quickly grows up to 15000% at around 3000 *rad/s*. In addition, bode plots of actuator dynamics are drawn as shown in [Fig. 11].

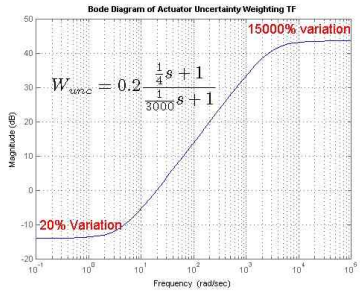

[Fig. 10] Uncertainty weighting TF

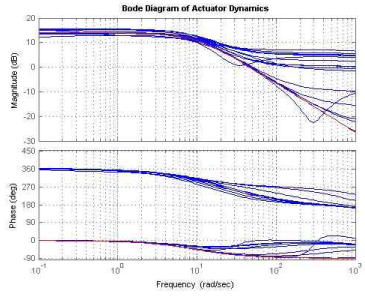

[Fig. 11] Bode plot of actuator dynamics

5.1 W_{perf1} Weighting Function Design: Case 1

The new TF, G_{actmod}, is designed as shown in Eq. 8 and corresponding uncertainty closed-loop transfer functions (CLTF) of x_1 and $x_1 - x_3$ are shown in [Fig. 12]. According to [Fig. 12], K_2 behaves better than K_1.

$$G_{actmod} = 5\frac{1}{\frac{1}{9.5}s+1}\left(1+\frac{0.2\left(\frac{1}{4}s+1\right)}{\frac{1}{3000}s+1}\triangle(s)\right). \quad (8)$$

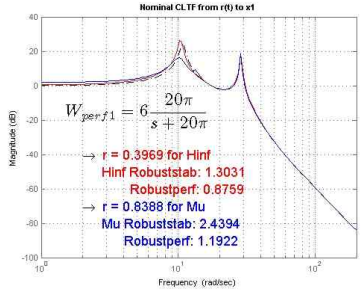

(a) System response of x_1

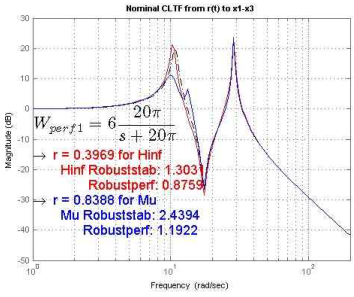

(b) System response of $x_1 - x_3$

[Fig. 12] System response of x_1 and $x_1 - x_3$ (case 1)

Particularly, in [Fig. 13(a)], the achieved H_∞ robust stability property value is 1.3031 which is larger than one and it means that the controller K_1 is stable. However, since the H_∞ robust performance property value, 0.8759, is less than one, it did not meet the requirement.

Again, GM and PM values are calculated as shown in <Table 5> and [Fig. 13].

<Table 5> PM and GM values of plant, CL_1, and CL_2

	Plant	CL_1	CL_2
GM (*dB*)	Inf	-2.63	Inf
PM (*deg*)	3.43	-0.782	2.84

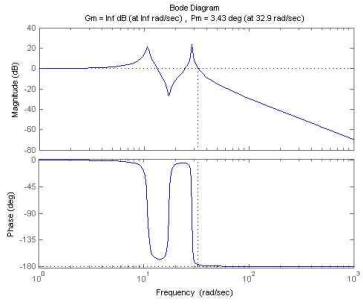

(a) Bode plot of plant

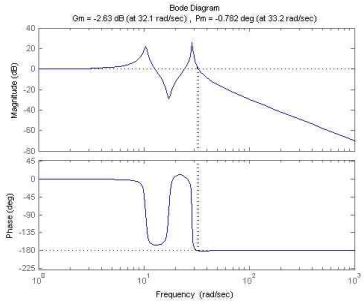

(b) Bode plot of CL_1

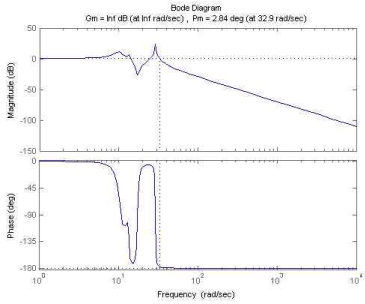

(c) Bode plot of CL_2

[Fig. 13] Bode plots of plant, CL_1, and CL_2

Unfortunately, PM value of CL_2 is even less than the PM value of the plant about 1 *deg*. CL_1 is even worse since both GM and PM values become negative. These results can be deduced from [Fig. 14]. Again, in order to compare the signal strength of three vibrations in detail, the third figure of [Fig. 14(a)] is redrawn in [Fig. 14(b)].

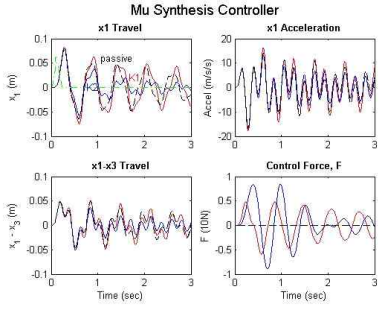

(a) System responses of x_1, $\ddot{x}_1$, x_3, and F

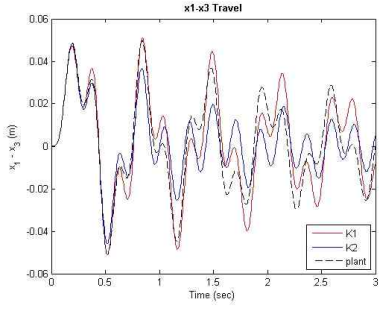

(b) System response of $x_1 - x_3$

[Fig. 14] System responses of μ-synthesis controller

According to [Fig. 14(b)], the K_1 controller vibrates even more than the plant, but the K_2 controller minimizes the magnitude of vibration. This can be interpreted as K_2 works better than K_1 in general.

RMS values of the plant, CL_1, and CL_2 are calculated as shown in <Table 6>.

<Table 6> RMS values of plant, CL_1, and CL_2

	Plant	CL_1	CL_2
RMS	8.4130	9.9588	8.2365

According to <Table 6>, CL_2 has the lowest RMS value, 8.2365, and it means that the vibration is the lowest among three curves in [Fig. 14(b)]. However, K_1 turns out to be even worse than the original plant. If we compare CL_2 values of <Table 4> and <Table 6>, the H_∞ controller works much better than μ-synthesis controller.

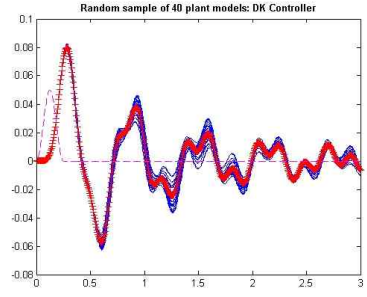

(a) 40 random samples of μ - synthesis controller

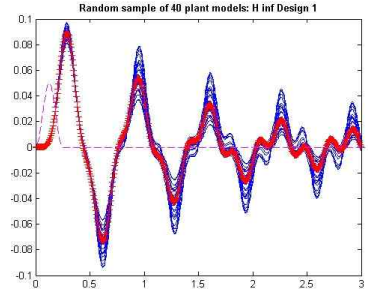

(b) 40 random samples of H_∞ controller

[Fig. 15] 40 random samples of μ-synthesis controller and H_∞ controller (case 1)

Now, random samples of 40 plant models are generated using both μ - synthesis controller and H_∞ controller as shown in [Fig. 15]. It is obvious that the vibration in [Fig. 15(b)] oscillates much more than the one in [Fig. 15(a)] and it means that μ-synthesis controller minimizes the vibration much more than H_∞ controller.

5.2 W_{perf1} Weighting Function Design: Case 2

By changing the W_{perf1} weighting function as

$$W_{perf1} = 10\frac{20\pi}{s+20\pi}, \tag{9}$$

resulting [Fig. 16], we can draw additional information. Here, the H_∞ robust stability property becomes less than one and it means that the controller is not stable ([Fig. 17(b)]). By looking at both [Fig. 15(a)] and [Fig. 17(a)], when the gain value of W_{perf1} is increased from six to ten, the oscillation of the random samples becomes stronger which is not good for the control design.

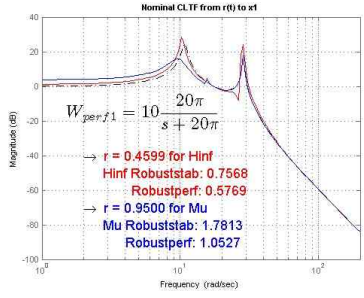

(a) System response of x_1

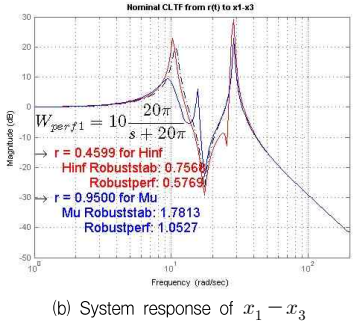

(b) System response of $x_1 - x_3$

[Fig. 16] System responses of μ-synthesis and H_∞ controller (case 2)

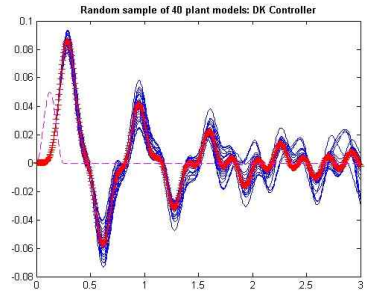

(a) 40 random samples of μ - synthesis controller

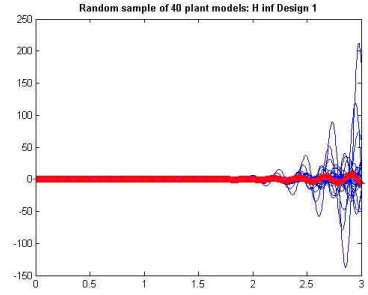

(b) 40 random samples of H_∞ controller

[Fig. 17] 40 random samples of μ-synthesis controller and H_∞ controller (case 2)

5.3 W_{perf1} Weighting Function Design: Case 3

Furthermore, changing the W_{perf1} weighting function as

$$W_{perf1} = 14\frac{20\pi}{s+20\pi}, \tag{10}$$

resulting [Fig. 18] and [Fig. 19] turns out to be even worse since the stability value is decreased from 0.7568 to 0.6361. However, in the aspect of μ-synthesis controller, the newly designed weighting function works better than before (much less vibration as shown in [Fig. 19(a)]).

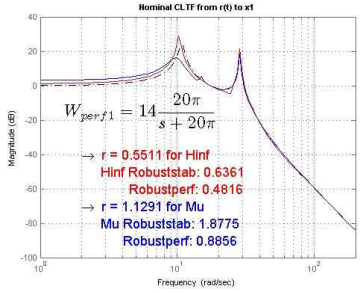

(a) System response of x_1

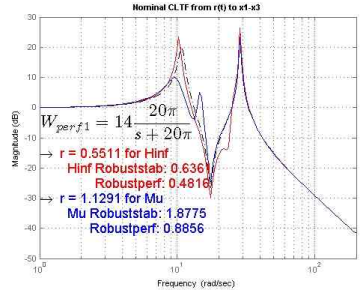

(b) System response of $x_1 - x_3$

[Fig. 18] System responses of μ-synthesis and H_∞ controller (case 3)

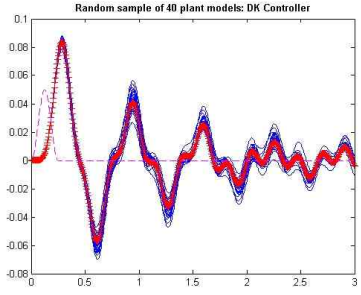

(a) System response of x_1

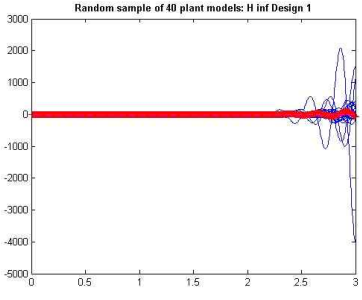

(b) System response of $x_1 - x_3$

[Fig. 19] System responses of μ-synthesis and H_∞ controller (case 3)

Finally, <Table 7> summarizes all the robust stability and robust performance property values of previous three cases of weighting functions.

<Table 7> Summary of the robust stability and performance values

		W_{perf1}		
		Case 1	Case 2	Case 3
H_∞	Robust Stab.	1.3031	0.7568	0.6361
	Robust Perf.	0.6759	0.5769	0.4816
μ-synthesis	Robust Stab.	2.4394	1.7813	1.8775
	Robust Perf.	1.1922	1.0527	0.8856

According to <Table 7>, it can be concluded that as robust stability value grows over one, the system becomes even more stable which can be deduced from [Fig. 15(a)], [Fig. 17(a)], and [Fig. 19(a)].

6. Conclusion

Through the paper, two kinds of controllers, including H_∞ controller and μ-synthesis controller are designed to control the motion of two masses in the given spring-mass- damper hardware system. Overall, the μ-synthesis controller controls the vibrations much better than the H_∞ controller and it is even much easier to design weighting functions using a μ-synthesis controller since it performs so stable. To design a more reliable controller, the user might use increased number of random samples rather than using only 40 random samples.

In the future, applications of the H_∞ controller and μ-synthesis controller to the quadrotor type unmanned aerial vehicle (UAV) will be studied based on the similar approach shown in this paper.

REFERENCES

[1] W. Ma and S. Lee, "Modelling and Development of Control Algorithm of Endoscopy," Journal of IT Convergence Society for SMB, Vol. 4, No. 2, pp. 33-39, 2014

[2] S. D. Cairano, A. Bemporad, I. V. Kolmanovsky, and D. Hrovat, "Model Predictive Control of Magnetically Actuated Mass Spring Dampers for Automotive Applications," International Journal of Control, Vol. 80, No. 11, pp. 1701-1716, 2007.

[3] Q. Gu and Y. Zhai, "Adaptive Model Predictive Control for SI Engines Fuel Injection System," Journal of the Korea Convergence Society, Vol. 4, No. 3, pp. 43-50, 2013.

[4] D. Karnopp, M. J. Crosby, and R. A. Harwood, "Vibration Control using Semi-Active Force Generators," Journal of Engineering for Industry, Vol. 96, No. 2, pp. 619-626, 1974.

[5] S. J. Dyke, B. F. Spencer, M. K. Sain, and J. D. Carlson, "Modeling and Control of Magnetorheological Dampers for Seismic Response Reduction," Smart Materials and Structures, Vol. 5, No. 5, pp. 565-575, 1996.

[6] L. M. Janson and S. J. Dyke, "Semiactive Control Strategies for MR Dampers: Comparative Study," Journal of Engineering Mechanics, Vol. 126, No. 8, pp. 795-803, 2000.

[7] D. Hrovat, P. Barak, and M. Rabins, "Semi-Active versus Passive or Active Tuned Mass Dampers for Structural Control," Journal of Engineering Mechanics, Vo. 109, No. 3, pp. 691-705, 1983.

[8] N. Varadarajan and S. Nagarajaiah, "Wind Response Control of Building with Variable Stiffness Tuned Mass Damper Using Empirical Mode Decomposition/ Hilbert Transform," Journal of Engineering Mechanics, Vol. 130, No. 4, pp. 451-458, 2004.

[9] J. You, K. You, and Y. Kim, "Aerodynamic Across-Wind Response for a Tall Building using Tuned Liquid Column Damper," International Conference on Convergence Technology, Vol. 2, No. 1, pp. 2035-2036, 2013.

[10] https://goo.gl/635c7I

[11] J. Gadewadikar, F. L. Lewis, L. Xie, V. Kucera,

and M. Abu-Khalaf, "Parameterization of All Stabilizing H_∞ Static State-Feeback Gains: Application to Output-Feedback Design," Automatica, Vol. 43, No. 9, pp. 1597-1604, 2007.

[12] G. Kopasakis, "Feedback Control Systems Loop Shaping Design with Practical Considerations," National Aeronautics and Space Administration, pp. 1-35, 2007.

[13] E. J. M. Geddes and I. Postlethwaite, "An H_∞ Based Loop Shaping Method and μ-Synthesis," Proceedings of the 30th Conference on Decision and Control, pp. 533-538, 1991.

[14] S. Rhee, "Comparison Study of H-infinity Controller Design Algorithms for Spacecraft Attitude Control," Journal of the Korean Society for Aeronautical and Space Sciences, Vol. 4, No. 1, pp. 57-69, 2016.

[15] J. Gadewadikar, H-infinity Output-Feedback Control: Application to Unmanned Aerial Vehicle, The University of Texas at Arlington, PhD Thesis, 2007.

[16] J. Kim, Mathematical Model for Dynamic Performance Analysis of Multi-Wheel Vehicle, Journal of the Korea Convergence Society, Vol. 3, No. 4, pp. 35-44, 2012.

[17] Y. Zhai, Stable Tracking Control to a Non-linear Process Via Neural Network Model, Journal of the Korea Convergence Society, Vol. 5, No. 4, pp. 163-169, 2014.

[18] T. Young and M. J. Mohlenkamp, Introduction to Numerical Methods and MATLAB Programming for Engineers, Ohio University, 2017.

저자소개

정 성 훈 (Sunghun Jung) [정회원]

- 2009년 8월 : 미네소타대학교 기계공학과 (공학학사)
- 2010년 12월 : 퍼듀대학교 기계공학과 (공학석사)
- 2013년 12월 : 퍼듀대학교 기계공학과 (공학박사)
- 2014년 1월 ~ 2016년 8월 : 삼성SDI 책임연구원
- 2016년 9월 ~ 현재 : 초당대학교 드론학과 조교수

<관심분야> : 무인항공기 자율기동, 에너지 효율적 경로 최적화, 배터리팩 상태예측 알고리즘 개발